The Importance of Nanometric Passivating Films on Cathodes for Li—Air Batteries

Brian D. Adams,[†] Robert Black,[†] Claudio Radtke,[†] Zack Williams,[†] B. Layla Mehdi,[‡] Nigel D. Browning,[‡] and Linda F. Nazar*[,†]

[†]Department of Chemistry and the Waterloo Institute for Nanotechnology, University of Waterloo, 200 University Avenue West, Waterloo, Ontario N2L 3G1, Canada and [‡]Fundamental and Computational Sciences Directorate, Pacific Northwest National Laboratory, P.O. Box 999, Richland, Washington 99352, United States

ABSTRACT Recently, there has been a transition from fully carbonaceous positive electrodes for the aprotic lithium oxygen battery to alternative materials and the use of redox mediator additives, in an attempt to lower the large electrochemical overpotentials associated with the charge reaction. However, the stabilizing or catalytic effect of these materials can become complicated due to the presence of major side-reactions observed during dis(charge). Here, we isolate the charge reaction from the discharge by utilizing electrodes prefilled with commercial lithium peroxide with a crystallite size of about 200—800 nm. Using a combination of S/TEM, online mass spectrometry, XPS, and electrochemical methods to probe the nature of surface films on carbon and conductive Ti-based nanoparticles, we show that oxygen evolution from lithium peroxide is strongly dependent on their surface properties. Insulating TiO_2 surface layers on TiC and TiN - even as thin as 3 nm—can completely inhibit the charge reaction under these conditions. On the other hand, TiC, which lacks this oxide film, readily facilitates oxidation of the bulk Li_2O_2 crystallites, at a much lower overpotential relative to carbon. Since oxidation of lithium oxygen battery cathodes is inevitable in these systems, precise control of the surface chemistry at the nanoscale becomes of upmost importance.

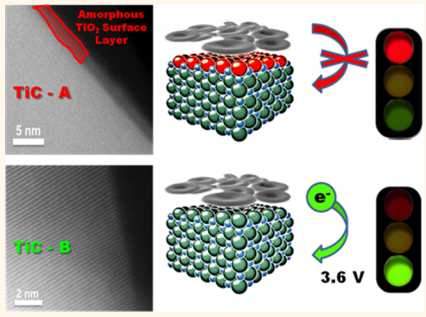

KEYWORDS: lithium oxygen batteries · lithium peroxide · cathodes · electrodes · surface passivation · electron transfer

Nonaqueous Li—O_2 cells (also referred to as Li—air batteries) based on the reversible formation of lithium peroxide have been the subject of intense investigation in the past few years.[1—4] Much fundamental work has been carried out to identify the reaction pathways of both discharge and charge of the cell.[5—7] However, complications arise in most studies due to the detrimental reactivity of most common electrolytes during discharge[8—12] and the known reactivity of carbonaceous positive electrode (cathode) materials on both discharge and charge.[13—15] Such studies and others have recently led to the introduction of noncarbonaceous electrode support materials such as Au,[16,17] TiC,[18] TiO_2,[19] and Al_2O_3-coated carbon fibers[15] in order to overcome the impedance owing to the formation of interfacial Li_2CO_3 *via* reaction of lithium peroxide with carbon.

Among the above, conductive titanium-based materials (i.e, TiN, TiC) are particularly attractive candidates for aprotic Li—O_2 cathodes. They have been utilized as alternative lightweight supports to carbon in electrodes for aqueous fuel cells and metal—air batteries due to their excellent oxidative stability.[20,21] Titanium nitride has been used in an acidic aqueous Li—air fuel cell and was found to have enhanced electrocatalytic activity for aqueous oxygen reduction relative to carbon.[22] Titanium nitride has also been used in the nonaqueous Li—O_2 battery,[23,24] but contrary to the study on TiC,[18] it has been used in combination with carbon, thus providing limited insight into its stability as a carbon replacement support material.

Surprisingly, little is understood regarding how the surface properties of these materials correlate to their performance, especially since the detrimental oxidation of carbon in the presence of super/per-oxide is known to be surface specific.[13,14] A very interesting recent discovery related to oxygen evolution, namely *via* photoelectrochemical water splitting on an n-type silicon

* Address correspondence to lfnazar@uwaterloo.ca.

Received for review September 19, 2014 and accepted November 3, 2014.

Published online November 03, 2014
10.1021/nn505337p

photoanode, provides an example. Work by Kenney *et al.*[25] demonstrates that ultra-thin passivating Ni/NiO_x films (<2 nm) on Si provide excellent photocurrent stability owing to their ability to only partially screen charge, whereas films >5 nm are ineffective.[25] Although the mechanism of the oxygen evolution reaction (OER) is quite different for photoelectrochemical-aqueous cells *vs* electrochemical-aprotic cells, this work nonetheless highlights the critical role of passivating surface films.

The above-mentioned reports have prompted us to examine how the cathode surface determines OER properties, by using a combination of transmission electron microscopy (TEM), X-ray photoelectron spectroscopy (XPS) and online electrochemical mass spectrometry (OEMS) in conjunction with electrochemical studies. Here, we report the results obtained on charging TiN and TiC electrodes prefilled with commercial Li_2O_2, and compare those to carbon, and also to cathodes that were electrochemically discharged. This has also allowed us to investigate how ORR side-reactions with the surface and electrolyte on discharge affect subsequent OER. We show that the specific surface nature of TiC plays a critical role in OER by either promoting or limiting charge transport, and that the inability to charge TiN electrodes relates solely to their extensive interfacial surface passivation by TiO_2. The extent of oxidation for carbon, TiC, and TiN is discussed in terms of thermodynamics and the outcome of this oxidation is the observed overpotential during charge. Facile electron transfer from the solid Li_2O_2, through a nanometric surface layer, and into the bulk of a conductive component in a Li−air cathode is the key to efficiency in this system.

RESULTS AND DISCUSSION

Titanium carbide (TiC) has been shown to be a highly promising electrode when coupled with a DMSO electrolyte, exhibiting enhanced stability and long-term cycling behavior that was ascribed to the formation of a passivating layer of TiO_2 on the surface.[18] In contrast, the only study of TiN as a single support material has demonstrated that it is effective for ORR, but it does not promote OER: this was suggested to be the result of poor electronic conductivity.[18] Although the study by Thiotyl *et al.* clearly proved that TiC is a promising cathode material, no comparisons were made to the carbon "standard" cathode in aprotic systems. In our work, we shed light on the underlying factors which enable the long-term cycling with TiC (and not TiN) and compare the OER performance to that of carbon.

The typical discharge−charge voltage profile for the first cycle of a Li−O_2 battery in LiTFSI/TEGDME with a carbon electrode is displayed in Figure 1a, to serve as comparison for the studies on the TiN and TiC

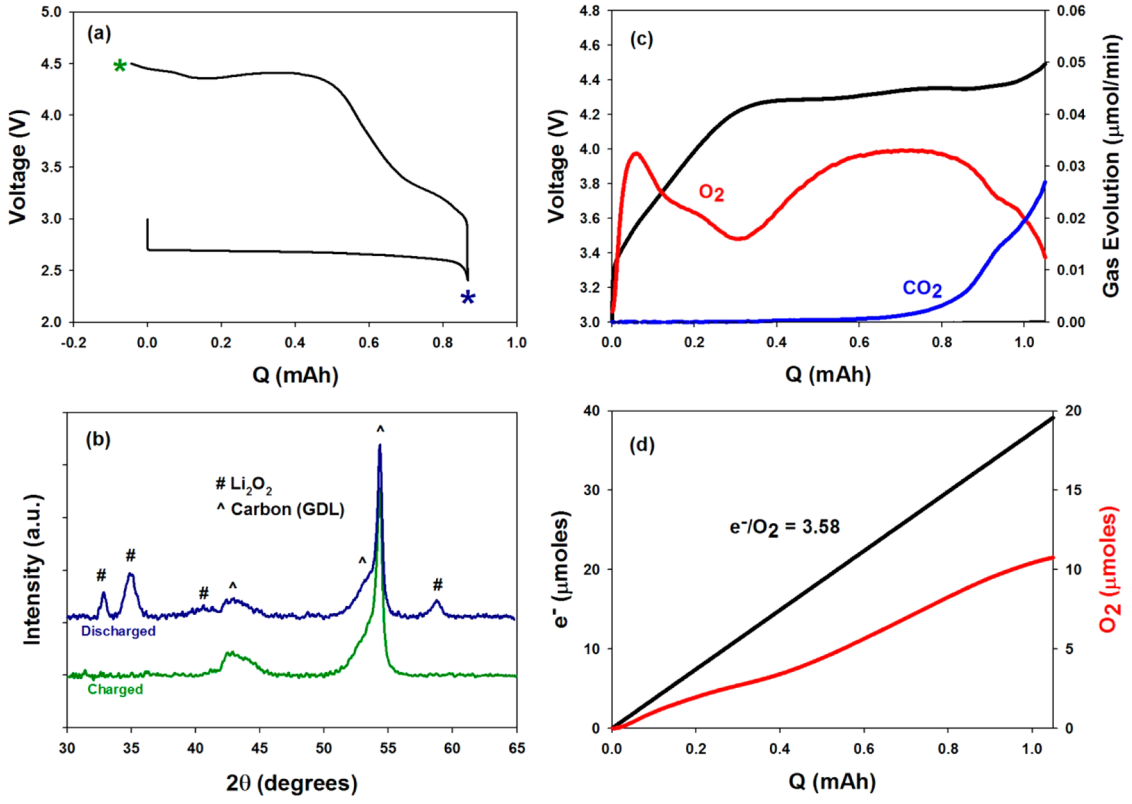

Figure 1. (a) Voltage profile of discharge/charge cycle with a Vulcan XC72 electrode at a current density of 25 μA/cm^2 in 1 M LiTFSI/TEGDME. (b) XRD patterns after discharge (Li_2O_2) and after charge (no Li_2O_2). (c) Gas evolution analysis with OEMS during the charge reaction (75 μA/cm^2) after discharging first to 1 mAh in O_2 (25 μA/cm^2). (d) The total integrated O_2 signal (m/z = 32) evolved from the cell in (c) along with the electrons passed. The overall e^-/O_2 ratio after full charge was 3.58.

electrodes. Powder X-ray diffraction of the electrode after discharge shows that Li_2O_2 is the sole crystalline product, and this is completely oxidized after charge (Figure 1b). Online electrochemical mass spectrometry (OEMS) was carried out to analyze the gases produced during the charge reaction after discharging in oxygen to 1 mAh (Figure 1c). The oxygen evolution profile occurs in two steps and a relatively large amount of CO_2 is evolved near the end of charge. The e^-/O_2 ratio is well above the expected value of 2 ($Li_2O_2 \rightarrow 2Li^+ + 2e^- + O_2$) throughout the charge process (Figure 1d). Quantification of the total amount of O_2 evolved after full charge to 1 mAh yields a value of 3.58 e^-/O_2. The CO_2 evolution indicates the oxidation of other compounds, including lithium carbonate, formate, and acetate, which are known to be the result of electrolyte decomposition during discharge.[8,39] Reactivity between the discharge intermediate LiO_2/O_2^- and the electrolyte salt[40,26] can also consume O_2 from the desired discharge product, contributing to the much less than theoretically presumed O_2 evolved on charge.

To disentangle the oxygen reduction (ORR) and evolution reactions (OER) and examine the oxidation reaction in isolation on charge, studies were carried out by charging cathodes that were prefilled with commercial Li_2O_2. This approach has been used by Shao-Horn *et al.*[27,28] to study the catalytic effect of adding various noble metals to carbon. Meini *et al.*[29] evaluated the charging characteristics of lithium peroxide and the possible discharge products (LiOH, Li_2CO_3, and Li_2O) on carbon. They found that Li_2O_2 is the only product that can be oxidized, and that it enhances oxidation of the electrolyte and the carbon support during charge.[30] We have also recently studied the Li_2O_2 oxidation mechanism, using *operando* X-ray diffraction, using both commercial peroxide powder and electrochemically deposited Li_2O_2.[31]

In the work reported here, we compare the XRD and OEMS results of electrochemically formed Li_2O_2 (discharged, Figure 1) to a Li−O_2 battery charge reaction which is isolated and independent from discharge by mixing commercial Li_2O_2 powder with the carbon support and then charging the electrodes. This eliminates any possibility of electrolyte decomposition on discharge. SEM images of the commercial Li_2O_2 powder and the composite electrode (Supporting Information Figure S1) reveal that the peroxide crystallite size is approximately 200−800 nm. Figure 2a shows the charging voltage profile for an electrode which was prefilled with Li_2O_2. The charge capacity was adjusted to an e^-/Li_2O_2 scale based on the mass of Li_2O_2

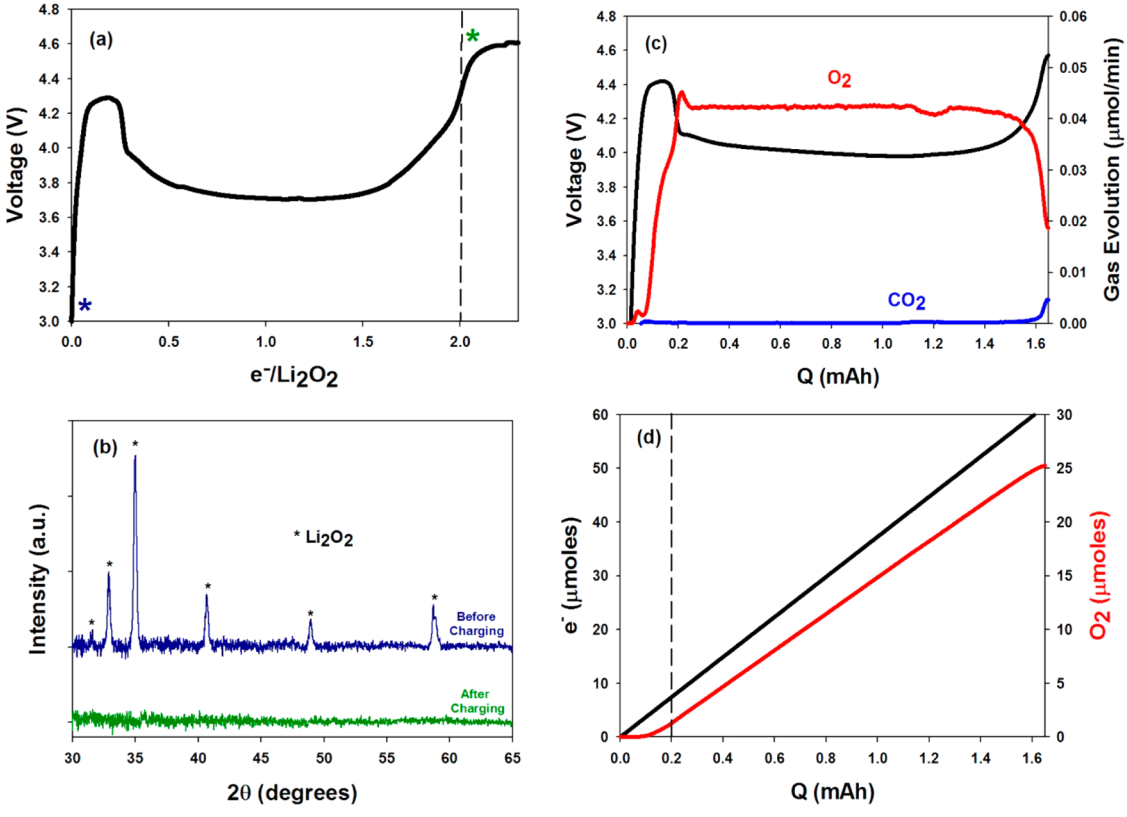

Figure 2. (a) The voltage profile for the charge reaction of a Li_2O_2-loaded Vulcan XC72 electrode at 50 $\mu A/cm^2$ in 1 M LiTFSI/TEGDME. (b) The XRD patterns of the composite electrode (Vulcan XC72 + Li_2O_2 + PTFE) before and after charging. (c) The gas evolution monitored by OEMS of a Li_2O_2-loaded Vulcan XC72 electrode charged at a current of 75 $\mu A/cm^2$. (d) The total integrated O_2 signal (m/z = 32) evolved from the cell in (c) along with the electrons passed. The overall e^-/O_2 ratio after full charge was 2.43.

contained in the electrode. The profile is defined by a high initial overpotential, followed by a plateau at approximately 3.7 V, and an eventual rise to 4.6 V (electrolyte oxidation voltage) after 2 e^-/Li_2O_2 is reached. The X-ray diffraction patterns of the initial electrode composite (carbon + Li_2O_2 + PTFE binder) show the characteristic peaks of the crystalline Li_2O_2 which completely disappear after charge (Figure 2b). OEMS analysis (Figure 2c,d) shows that oxygen starts to evolve mainly after the initial overpotential is surpassed. The total e^-/O_2 is 2.43 after full charge, not the theoretically expected 2.0.

Both the voltage profile and gas evolution are similar to what has been observed previously.[30,32] The chemical reactivity of Li_2O_2 and carbon is well-known to form carbonates and epoxy groups.[13,14,33] This reaction at the Li_2O_2/carbon interface also causes interfacial resistance[33] and is responsible for the observed overpotential. Meini *et al.* carefully studied this "electrode activation" process with prefilled carbon electrodes and conclude that the cause of this initial overpotential is the result of carbon/Li_2O_2 interfacial resistance rather than LiOH or Li_2CO_3 surface layers on the Li_2O_2 particles.[32] A ^{13}C electrode was used in our studies to distinguish between carbon electrode oxidation ($^{13}CO_2$) and electrolyte decomposition ($^{12}CO_2$). CO_2 from both sources is evolved near the end of charge (Supporting Information Figure S2), but its evolution from the carbon electrode dominates at the higher potentials owing to carbon corrosion. Obviously, there is a miniscule amount of $^{12}CO_2$ evolved at the early stage of charge and more at the end as the voltage increases. This is attributed to a superoxide-rich surface of the Li_2O_2 during charge reacting with the electrolyte.[31,34] The decomposition products are oxidized to CO_2 as the voltage increases at the end of the charge process. The relatively flat voltage profile on charging carbon electrodes prefilled with peroxide with an e^-/O_2 ratio of 2.43, compared to the sloping charge profile of electrodes that have undergone electrochemical discharge (e^-/O_2 = 3.58) furthermore suggests that side reactions on discharge are more important than previously thought. The relative amounts of Li_2O_2 in the electrodes after discharge (Figure 1) compared to those prefilled with Li_2O_2 (Figure 2) prior to charging are displayed in Supporting Information Table S1. The electrochemical discharge product contains ~82% Li_2O_2, which is similar to that of the electrodes prefilled with commercial Li_2O_2 (~85%). However, the difference in evolved gases (CO_2 and O_2) during charge indicates that the impurities in the commercial powder are much different than what is formed *via* electrolyte decomposition during electrochemical discharge. Specifically, the nature of these side products is confirmed to be mainly LiOH (where no CO_2 evolution is observed) for the commercial Li_2O_2 as previously reported[28] and formate, acetate, and carbonates in the electrochemically discharged electrodes (where CO_2 is evolved).[8] The fact that <100% of the theoretical amount of O_2 is evolved (82%) for prefilled electrodes, however, indicates that the electrolyte/electrode surface reacts with Li_2O_2 during oxidation. The current density on charge also strongly affects the potential for Li_2O_2 oxidation, as expected. The voltage plateau is at 3.7 V (Figure 2a) and 4.0 V (Figure 2c) for applied current densities of 50 $\mu A/cm^2$ and 75 $\mu A/cm^2$, respectively. The poor contact of the Li_2O_2 crystallites with the support as well as their larger particle size[29] also undoubtedly contributes to the initial high charging potentials compared to the "electrochemically loaded" electrode.

Turning to the noncarbonaceous electrodes, the activity of TiN for ORR/OER was probed using both half-cell (three electrode) studies and full cells (two electrodes). The results of the half-cell study employing chronoamperometry for ORR and linear sweep voltammetry for OER on a TiN film are shown in Supporting Information Figure S3. They suggest that although oxygen reduction readily occurs, oxygen evolution does not. This was confirmed by full cell studies shown in Figure 3a, which demonstrate a voltage profile similar to that presented by Thotiyl *et al.* for a TiN electrode.[18] Li_2O_2 is formed on discharge, but it remains even after charging to 4.8 V (Figure 3b) as shown by XRD. A Li_2O_2-loaded TiN electrode gives the same result as the cell examined on discharge and charge (Figure 3c,d), suggesting a path toward a simplified screening process of support materials suitable for OER in the Li−O_2 battery using these prefilled electrodes. The underlying cause of this lack of OER capability was examined by comparison of TiN with Vulcan carbon using electrochemical impedance spectroscopy (Supporting Information Figure S4). The charge transfer resistance increases for both electrodes during the course of discharge owing to the accumulation of insulating Li_2O_2.[5] On switching to an anodic polarization of the electrode, a drastic increase in the charge transfer resistance is observed for TiN, indicating substantial oxidation of the nitride surface in the presence of Li_2O_2. This causes the voltage to rise to 4.7 V, with this upper limit thus ending charge. This is analogous behavior to that observed in aqueous media. Avasarala and Haldar report that the nitride surface becomes passivated by hydroxide groups at elevated temperature which reduces its electrical conductivity, thereby inhibiting its electron transportation properties.[35] In contrast, the impedance for the carbon electrode remains the same on anodic polarization, in accord with the fact that carbon is capable of fully charging below 4.7 V.

With the idea that surface oxidation of Ti-based materials is the factor that determines the ease of electron transfer between Li_2O_2 and the support on charge, we examined other commercial Ti-based oxide

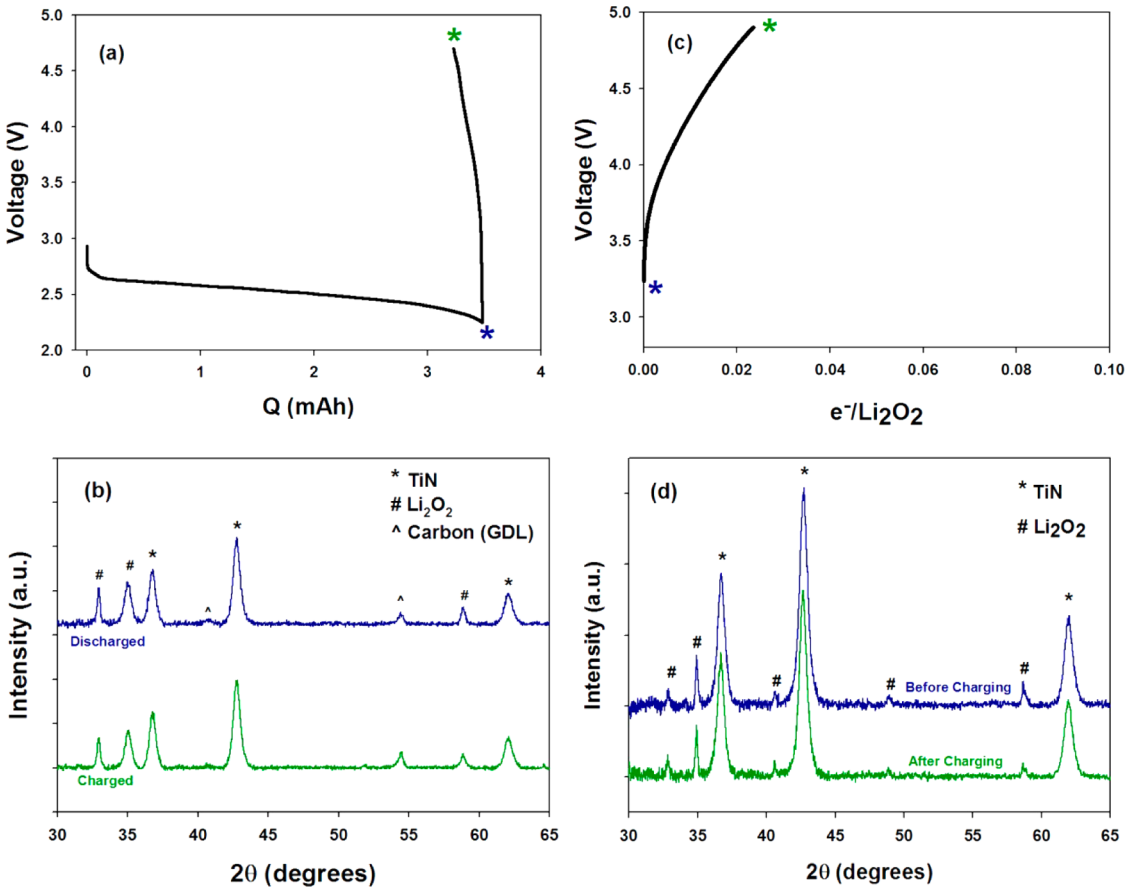

Figure 3. (a) The voltage profile of a TiN electrode discharge and charged at a current density of 25 μA/cm^2 in 1 M LiTFSI/TEGDME. (b) The XRD patterns of the electrode after discharge and charge. Li_2O_2 is present after discharge and remains after charge. (c) The voltage profile for the charge reaction of a Li_2O_2-loaded TiN electrode at 50 μA/cm^2 in 1 M LiTFSI/TEGDME. (d) The XRD patterns of the composite electrode (TiN + Li_2O_2 + PTFE) before and after charging.

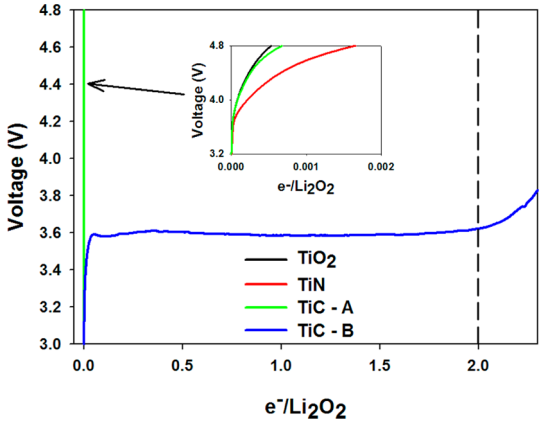

Figure 4. Voltage profiles of Li_2O_2-loaded TiC-A, TiC-B, TiN, and TiO_2 electrodes which were charged in 1 M LiTFSI/TEGDME at current densities of 50 μA/cm^2. Of these electrodes, only TiC-B was capable of oxidizing Li_2O_2.

and carbide support materials. Figure 4 shows the charge curves for anatase TiO_2, and two different TiC nanopowders (TiC-A and TiC-B, obtained from two different suppliers), compared to TiN. As expected, the (poor) semiconducting TiO_2 electrode (fully oxidized) did not support OER, similar to TiN discussed above, as a result of its completely "insulating" bulk and surface. Surprisingly, however, one TiC material promoted OER whereas the other did not. TiC-A was inactive for OER, but the voltage profile of TiC-B exhibits a very flat plateau at 3.6 V corresponding to the oxidation of Li_2O_2. This appears complete at the expected ratio of 2 e^-/Li_2O_2, where beyond this point, the upturn in voltage suggests that other oxidation processes (*i.e.*, electrolyte side reactions) occur. It is interesting to note that the profile is very different compared to that reported for the full cycling of TiC in DMSO as reported by Thiotyl *et al.*, namely, a charge curve that exhibits a very pronounced slope from 3.0 to 4.0 V.[18] The higher initial oxidation voltage in the prefilled cathode studied here is partly a consequence of the electrode−Li_2O_2 contact as explained above; the flat charging voltage observed here indicates that oxidation of electrochemically peroxide-loaded TiC (*i.e.*, from discharged cells as reported elsewhere)[18] involves additional processes than those involving Li_2O_2 alone. These could be derived from oxidation of $Li_{2-x}O_2$ that would occur at a lower potential, and/or electrolyte reactivity.

OEMS analysis of a Li_2O_2-loaded TiC-B electrode resulted in a similar gas evolution profile compared to the carbon-based electrodes, but with no initial lag

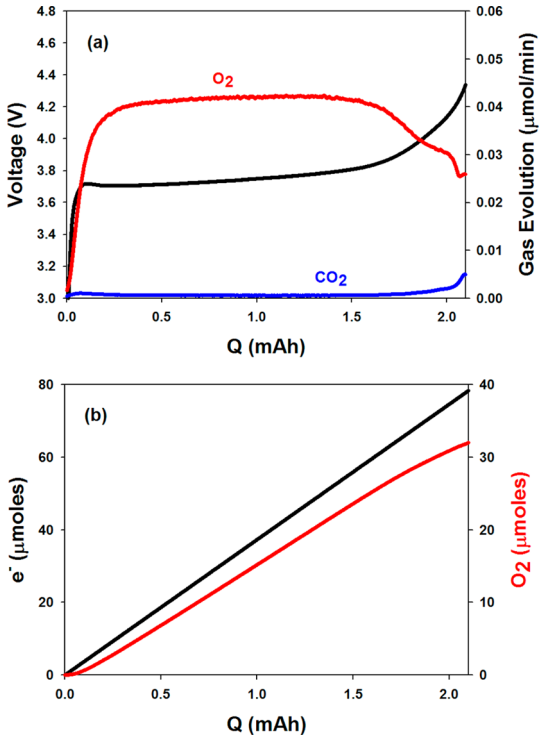

Figure 5. (a) The gas evolution monitored by OEMS of a Li_2O_2-loaded TiC-B electrode charged at a current density of 75 μA/cm^2. (b) The total integrated O_2 signal (m/z = 32) evolved from the cell in (a) along with the electrons passed. The overall e^-/O_2 ratio after full charge was 2.45.

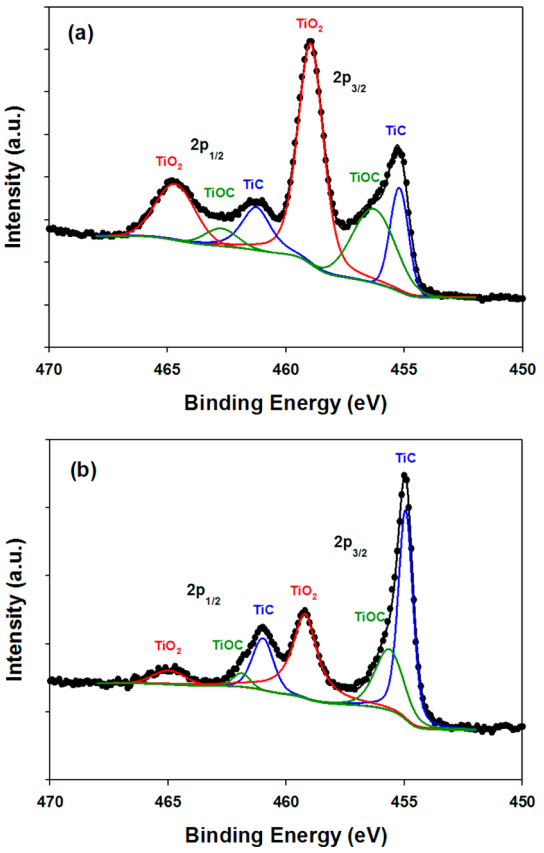

Figure 6. Ti 2p XPS spectra for (a) TiC-A nanopowder and (b) TiC-B nanopowder.

in O_2 evolution or overpotential (Figure 5). The overall e^-/O_2 ratio after full charge was 2.45. The reaction between Li_2O_2 and the electrolyte on charge in the case of TiC is identical to that on carbon (accounting for an e^-/O_2 of 2.43 *vs* 2.45 for carbon and TiC, respectively), but again, is clearly not as significant as the reactivity which occurs on discharge in the case of carbon electrodes as shown in Figure 1c,d. On the basis of this, as well as the minor CO_2 evolution at the end of charge, we conclude that electrolyte decomposition is a factor on both discharge and charge but the support material has a much lesser effect, indicating a solution-phase reaction rather than electrode surface reactivity. In an attempt to shed light on the outstanding cycling behavior of the TiC/DMSO system studied by Thiotyl *et al.*,[18] we compared the OEMS analysis for Li_2O_2-loaded TiC-B electrodes in TEGDME and DMSO electrolytes (Supporting Information Figure S5). Unfortunately, the voltage for Li_2O_2 oxidation was higher in DMSO than in TEGDME and was accompanied by less O_2 evolution and more CO_2 evolution.

Our studies of the two TiC nanocrystallite materials indicate that their bulk properties are identical, but the nature of their surface is quite different. The XRD patterns for TiC-A and TiC-B show that they both have similar crystallinity and the SEM images show that the morphology and particle size distribution are identical (Supporting Information Figure S6). The BET surface area of these two materials as determined by N_2 adsorption experiments was the same (24 and 26 m^2/g for TiC-A and TiC-B, respectively), as were the bulk conductivities determined by the four-point probe technique (73 and 75 S/cm for TiC-A and TiC-B, respectively). However, the surface of the materials, examined by X-ray photoelectron spectroscopy (XPS), reveals distinct differences. The XPS data displayed in Figure 6 clearly shows that the TiC-A surface is TiO_2-rich, whereas the TiC-B is TiC-rich. The surface ratios of TiC/TiOC/TiO_2 are 0.22:0.23:0.55 and 0.45:0.21:0.34 for the TiC-A and TiC-B, respectively, determined by the areas under the fitted Ti 2p peaks in the XPS spectra. We conclude that, as in the case of TiN (Supporting Information Figure S7), the dominance of insulating TiO_2 on the surface of TiC-A inhibits electron transfer from Li_2O_2 during charge. Noteworthy is the fact that the XPS spectrum of "inactive" TiC-A is virtually identical to that reported for "active" but passivated TiC formed on cycling,[18] suggesting that the nature of the interfacial contact is more complex than revealed by XPS spectra alone. Furthermore, although the surface of TiC-B consists predominantly of TiC (45%), there are still contributions of TiO_2 (34%) and TiOC (21%). This means that the surface layer (TiO_2/TiOC) is either extremely thin or nonhomogenous.

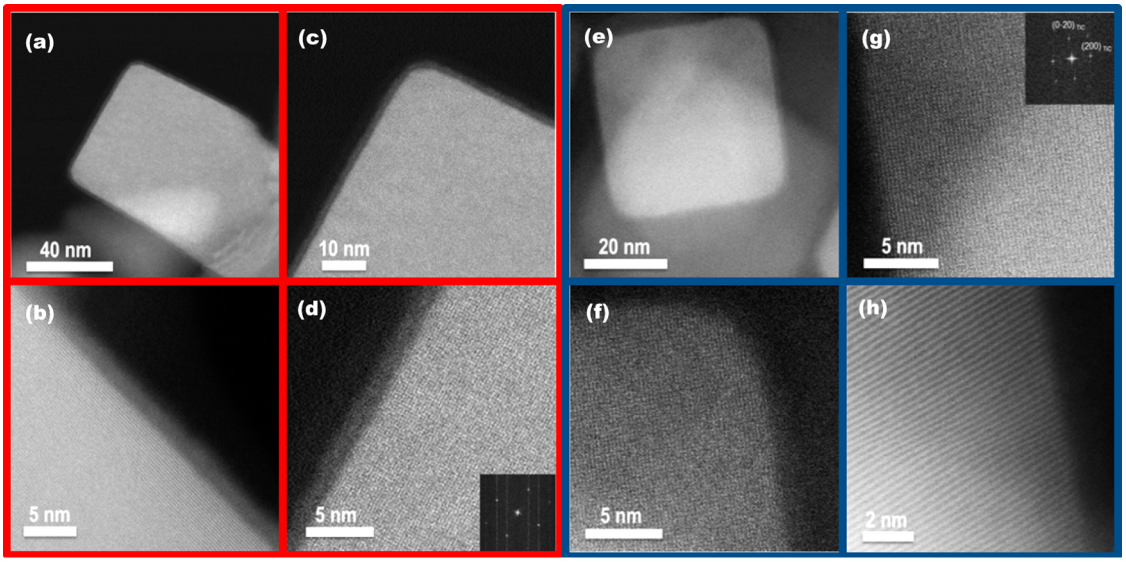

Figure 7. (S)TEM images of individual nanocrystallites of TiC-A (a–d) and TiC-B (e–h). The insets in (d) and (g) show the corresponding SAED patterns of TiC-A and TiC-B, respectively.

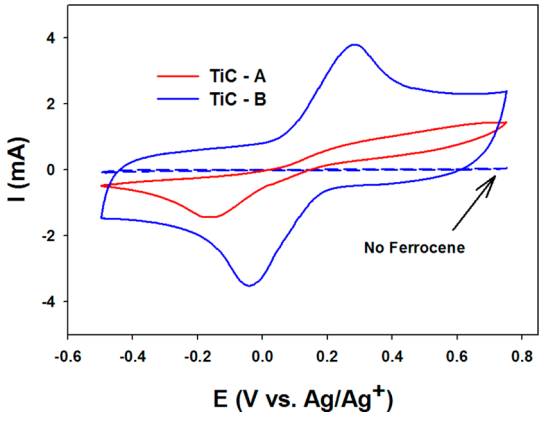

Figure 8. Cyclic voltammograms at a scan rate of 100 mV/s in 0.1 M TBAP/MeCN + 3 mM ferrocene on electrodes made from TiC-A (red) and TiC-B (blue). The dashed line is a voltammogram in the supporting electrolyte only on TiC-B (*i.e.*, 0.1 M TBAP/MeCN) to show that the activity is entirely due to the Fc/Fc^+ redox couple.

This surface layer was further examined by scanning transmission electron microscopy, (S)TEM, as shown in Figure 7. The TiC-A crystallites are characterized by an amorphous layer which completely surrounds the particles and is approximately 2–3 nm thick (Figure 7b–d). However, no surface layer can be observed on the TiC-B particles (Figure 7e–h). Lattice fringes extend to the outer edge of the particle even at the highest magnification (Figure 7h).

Electron transfer on these two TiC nanocrystallite materials was probed with the ferrocene (Fc) solution-based redox couple (Figure 8). TiC-B presented a reversible Fc/Fc^+ couple, whereas the TiC-A exhibited an ill-defined oxidation peak with reduction far from its kinetically reversible position. We have found this behavior for a variety of insulating electrode materials where the oxidation of ferrocene is slow and not kinetically reversible due to poor electron transfer rates. Electron transfer with the TiC-A is inhibited by its insulating surface layer and TiC-B (that lacks an impeding surface layer) displays fast electron transfer kinetics. The $TiOC/TiO_2$ surface coating on the TiC-A particles can be removed by vacuum annealing at 300 °C, providing sufficient electron transfer properties (Supporting Information Figure S8). On the other hand, it is difficult to oxidize the TiC-B material at ambient temperature, indicating that the surface oxide layer on TiC-A must be a result of the conditions used for its commercial production.

Although both TiN and TiC are used in practical applications due to their oxidation resistance,[21] there has been much work on comparing the oxidation resistance between these two materials.[36,38] The oxidation reactions of these materials with oxygen are displayed in eqs 1[20] and 2[37].

$$2TiN + 2O_2 \rightarrow 2TiO_2 + N_2$$

$$\Delta G^\circ = -611.8 \text{ kJ mol}^{-1} \text{ (298 K)} \quad (1)$$

$$TiC + 2O_2 \rightarrow TiO_2 + CO_2$$

$$\Delta G^\circ = -551 \text{ kJ mol}^{-1} \text{ (298 K)} \quad (2)$$

In the work of Komratov,[38] it was shown that TiC oxidizes more slowly than TiN in air, and this was attributed to the formation of a protective oxide film on TiC which inhibits further oxidation. This is in complete accord with the Gibbs free energies for these reactions (*i.e.*, the oxidation of TiN is more favorable than TiC). The Gibbs free energy for the oxidation of carbon (graphite) by molecular oxygen is only -394.4 kJ mol^{-1} at 298 K ($C + O_2 \rightarrow CO_2$). This is unlikely to occur under the

conditions of the Li−O_2 battery, and as such it has been shown that other products are indeed formed, including Li_2CO_3, from direct reaction between carbon and Li_2O_2 eqs 3 and 4.[33]

$$C + Li_2O_2 + 1/2O_2 \rightarrow Li_2CO_3$$
$$\Delta G^\circ = -542.4 \text{ kJ mol}^{-1} \text{ (300 K)} \quad (3)$$

$$C + Li_2O_2 \rightarrow Li_2O + Li_2CO_3$$
$$\Delta G^\circ = -533.6 \text{ kJ mol}^{-1} \text{ (300 K)} \quad (4)$$

Determining the oxidation resistance of a material is obviously more complex than the simple thermodynamics, although this can act as a preliminary guideline. On the basis of our results, the facile oxidation of TiN is clear. The thermodynamics tell us that this is reasonable, given the greater free energy for this reaction (−611.8 kJ mol^{-1}). The Gibbs free energies for the oxidation of TiC *vs* carbon are close (−551 *vs* −542.4 kJ mol^{-1}). In agreement with Komratov,[38] when the starting TiC material lacks an oxide layer (TiC-B), any surface film that forms during the charge process is thin enough to inhibit further oxidation and still allows for facile electron transfer. The observed voltage for OER from Li_2O_2 for carbon electrodes is slightly higher than that of TiC-B. This is likely due to the defective nature of carbon and surface functional groups, which leads to oxidation products such as epoxy groups and carbonates.[14]

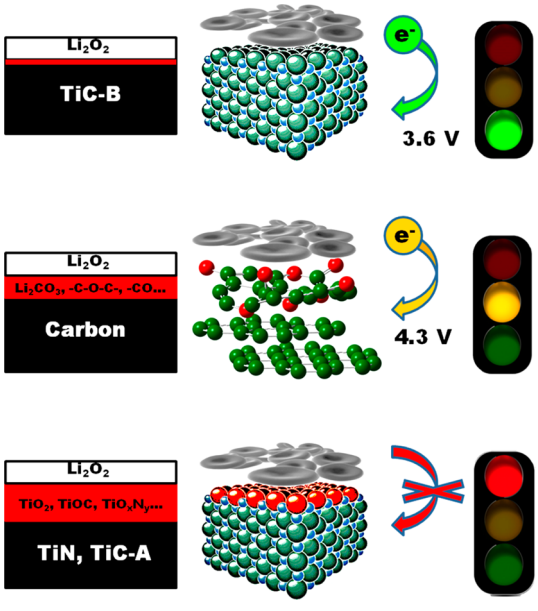

Scheme 1. Concept of Li_2O_2 oxidation on the various materials examined in this study. Electron transfer from Li_2O_2 to the bulk TiC-B occurs readily with a very thin passivating TiO_2/TiOC surface as evidenced by XPS and (S)TEM. The surface of carbon is oxidized to form carbonates, epoxides, and carbonyl groups which still allows for electron transfer, but with a substantial charging overpotential. On the TiN and TiC-A, the thick insulating TiO_2/TiOC/TiO_xN_y surfaces completely inhibit electron transfer.

The results above are summarized in Scheme 1. Electron transfer from Li_2O_2 through insulating surface layers on conductive materials plays the most critical role in the charge reaction of the nonaqueous Li−O_2 battery. If the passive surface layer is thin enough (TiC-B), Li_2O_2 can be easily charged at a constant voltage. In fact, such an ultrathin passivating layer undoubtedly stabilizes the material on cycling, as previously proposed.[18] In the case of slightly thicker or more insulating surfaces (*i.e.*, oxidized carbon), charging can still occur, but an overpotential needs to be overcome. If the surface layer is too thick (TiN and TiC-A), electron transfer that is critical to the charging process is inhibited. In the case of TiC, an oxide layer of even 2−3 nm (Figure 7) is enough to completely prohibit electron transfer. This critical thickness is meaningful in the consideration of oxidation resistant materials for cathodes for the Li−O_2 battery.

CONCLUSIONS

Although bulk conductivity is required for electron transfer to promote oxidation of lithium peroxide on cathode supports for the Li−O_2 battery, the surface chemistry of the support is most critical in determining the efficiency of electron transfer to the insulating Li_2O_2 during the charge reaction. In this study, we have confirmed that carbon electrodes react directly with Li_2O_2, causing an overpotential on charge due to an oxidized, high impedance surface. The surface of TiN is fully oxidized by Li_2O_2 when an anodic current is applied, to the extent where electron transfer is inhibited and the charge reaction is halted. Obviously, TiN is not as oxidatively stable as TiC. Thin surface layers of insulating TiO_2 on TiC (*i.e.*, TiC-A) also inhibit the charge reaction, but TiC which lacks this surface layer or where the layer is thinner than the critical value of 2 nm (*i.e.*, TiC-B) facilitates Li_2O_2 oxidation with a greatly decreased overpotential. Oxidation of the solid and insulating Li_2O_2 product in the nonaqueous Li−O_2 battery is a sluggish reaction and sensitive to the applied current rates. Precise control of passivating surface layers will be a significant breakthough in research on the aprotic Li−O_2 battery system.

This study also shows that the main effect of material variation in cathodes for the Li−O_2 battery is the voltage at which Li_2O_2 is oxidized, rather than changes in O_2/CO_2 evolution. This indicates that electrolyte decomposition probably occurs at the Li_2O_2 surface, but is somewhat independent of the nature of the cathode. Bulk conductivity is required, yet surface conductivity is of equal importance and the Li_2O_2 charging voltage is directly related to the nature of surface layers (thickness and conductivity). Under the harsh conditions of the cell, it is expected that surface oxidation will always occur. However, new cathode

materials can now be designed such that their surfaces inhibit excessive oxidation (leading to an insulating oxide) and/or are concealed by conductive oxide layers.

METHODS

Preparation of Gas Diffusion Electrodes. In the cases where cells were discharged, typical gas diffusion electrodes were prepared by casting an active layer on a gas diffusion layer as described in previous publications.[5,39] Briefly, Vulcan XC72 (Cabot Corp.) or titanium nitride nanopowder (<20 nm, >97%, Nanostructured and Amorphous Materials, Inc.) were mixed with PTFE in a ratio of 4:1 and films were cast onto Toray carbon paper (TGP-H-030, Fuel Cell Store). These sheets were first dried at 90 °C for 1 h and then annealed for an additional hour at 300 °C under vacuum. After cooling, electrodes were punched (1 cm^2 area).

Preparation of Li_2O_2-Loaded Electrodes. Lithium peroxide (90%, Sigma-Aldrich) was used as received. The actual purity of this powder was determined to be 88% by iodometric titration, using a modified method of what has been previously reported in the literature[40] (see Supporting Information for details). The e^-/Li_2O_2 ratio, calculated by the electrical charge passed and the mass of Li_2O_2 in the electrode, was adjusted based on this value of purity. In an argon-filled glovebox, the Li_2O_2 powder was hand-mixed with Vulcan XC72 (Cabot Corp.), TiN (titanium nitride nanopowder <20 nm, >97%, Nanostructured and Amorphous Materials), TiO_2 (titanium(IV) oxide, anatase nanopowder, <200 nm, 99.7%, Aldrich), TiC-A (titanium(IV) carbide nanopowder, <200 nm, 95%, Aldrich), or TiC-B (titanium carbide nanopowder, <25 nm, 99+%, US Research Nanomaterials) and a PTFE dispersion in 2-propanol. The resulting paste was spread onto Ti mesh (100 mesh, Alfa Aesar) disk substrates (1 cm^2). Stainless steel disks (100 mesh, 316 grade) were used as substrates for the DEMS studies. These formed electrodes were finally dried at room temperature under vacuum. The mass ratios of carbon:Li_2O_2:PTFE and TiX:Li_2O_2:PTFE were 4:1:1 and 4:0.5:1 in all cases.

Galvanostatic Discharging/Charging. Galvanostatic (dis)charging of the gas diffusion electrodes or Li_2O_2-loaded electrodes was carried out using a modified Swagelok design with 1 M lithium bis(trifluoromethanesulfonyl)imide (LiTFSI, Novolyte) in tetraethylene glycol dimethyl ether (TEGDME, 99%, Sigma-Aldrich, redistilled) as the electrolyte. The water content of the electrolyte was <1 ppm as determined by the Karl Fischer titration method with a C30 Coulometer (Mettler Toledo). Cells were assembled in an argon filled glovebox with a lithium metal counter electrode, three porous separators (Millipore glass fiber), and the as-prepared Li_2O_2-loaded (or gas diffusion) electrodes as the working electrodes. The electrolyte (200 μL) was added to the separators during cell assembly. The cells were equilibrated at open circuit for 6 h before testing and were controlled with a BT2000 battery cycler (Arbin Instruments). All cells were charged at room temperature (25 ± 2 °C). In the case of the cells which were discharged, O_2 was introduced through a quick connect gas line system with Swagelok fittings and metal tubing. An excess volume of O_2 was stored in a headspace (an aluminum tube above the cathode) at a pressure of 1.5 atm. For all Li_2O_2-loaded electrodes, galvanostatic charging was performed under an argon atmosphere.

Characterization. Powder X-ray diffraction was performed using a Bruker D8-Advance powder diffractometer with Cu−$K_{\alpha 1}$ radiation (λ = 1.5405 Å). Scanning electron microscopy (SEM) samples were imaged using a LEO 1530 field-emission SEM. Nitrogen adsorption was measured using a Quantachrome AUTOSORB-1 system and the Brunauer−Emmett−Teller (BET) method was utilized to calculate the surface area. The TiC-A and TiC-B samples were pressed into 13 mm diameter pellets of approximately 0.5−1 mm thick. A Jandel multi height four-point probe combined with a RM300 test unit was used to measure the resistivity which was subsequently converted to values of bulk conductivity. XPS analysis was performed on a Thermo ESCALAB 250 instrument configured with a monochromatic Al Kα (1486.6 eV) source. All spectra were fitted with Gaussian−Lorentzian functions and a Shirley-type background using XPSPEAK software. The binding energy values were calibrated using the C *1s* peak at 285.0 eV. The (S)TEM images TiC-A and TiC-B used in this study were acquired with a FEI Titan aberration-corrected scanning transmission electron microscope (STEM) operated at 300 kV and equipped with CEOS GmbH double-hexapole aberration corrector for the probe-forming lens, which allows imaging with ~0.1 nm resolution STEM mode.

Online Electrochemical Mass Spectrometry (OEMS). The residual gas analysis was performed with a modified design based on an OEMS apparatus reported by Tsiouvaras *et al.*[41] A commercial electrochemical flow cell (EL-Cell, ECC-DEMS) was attached in-line with a gas flow controller (Bronkhurst, F-200CV) and a quadrupole mass spectrometer (Stanford Research Systems, RGA 200). The cell (and all regular Swagelok cells used for galvanostatic (dis)charging) was leak tested under O_2 pressure using a high accuracy pressure transducer to measure any pressure drop (Omega PX409-USBH), and found to be hermetically sealed. During cell operation a controlled flow of Ar (5.0 grade) sweeps the evolved gases from the cell to the MS entrance chamber where the gas enters the quadrupole through a fused silica capillary (50 μm i.d.). The pressure inside the MS chamber was 3×10^{-6} Torr during operation. Prior to measurement, the mass spectrometer was calibrated to establish a relationship between the measured ion current (A) and target gas concentration (ppm). With the use of known gas concentrations (from 2000 ppm of O_2/Ar balance and 2000 ppm of CO_2/Ar balance mixtures) mixed with different amounts of Ar, a linear relationship between the gas concentration and ion current was established. The quantification was performed with the use of Mathworks Matlab software.

Nonaqueous Electrocatalytic Studies. Catalyst inks were prepared by homogeneously dispersing TiN nanopowder in 1 mL of NMP solution containing Li^+-ion exchanged Nafion (Nafion-Li).[5,42] Dispersions were prepared with a Nafion-Li/TiN mass ratio of 1:2. A glassy carbon electrode (Pine Instruments, Co., 0.196 cm^2) was coated with the ink and dried at 100 °C for 24 h to obtain coating loads of 250 μg TiN/cm^2. The electrochemical experiments were performed in an argon-filled glovebox, with a three-electrode cell gas-flow enabled setup consisting of the coated glassy carbon electrode as the working electrode and Li foil as both the counter and reference electrodes. Cyclic voltammetry, chronoamperometry, and linear sweep voltammetry experiments were controlled with a VMP3 potentiostat and EC-Lab software (Bio-Logic Science Instruments). The electrolyte used was 0.1 M lithium hexafluorophosphate ($LiPF_6$, Novolyte) in TEGDME, and all experiments were performed at room temperature.

Electrochemical Impedance Spectroscopy. Impedance measurements were performed using a VMP3 potentiostat/galvanostat with EIS/Z capabilities and EC-Lab software (Bio-Logic Science Instruments). The DC voltage was maintained at open-circuit and an AC voltage was applied with an amplitude of 5 mV from 300 kHz to 50 mHz.

Ferrocene Experiments. Cyclic voltammetry was performed with a three-electrode cell gas-flow enabled setup. The working electrodes were prepared by painting mixtures of TiC-A or TiC-B and PTFE dispersions in 2-propanol onto stainless steel mesh disks (316 grade, 1 cm^2) with Ti wire leads such that the mass ratio of TiC/PTFE was 4:1. The counter electrode was Pt gauze (3 cm^2) and a Ag/Ag^+ (0.01 M $AgNO_3$ + 0.1 M TBAP in MeCN) reference electrode was used. A solution of 0.1 M tetrabutylammonium perchlorate (TBAP, ≥ 99.0%, Fluka) in acetonitrile (MeCN, anhydrous HPLC grade, 99.8%, Caledon) with 3 mM ferrocene constituted the electrolyte. The ferrocene (98%, Aldrich) was purified by sublimation at 110 °C prior to use. Argon was bubbled through the electrolyte solution before and over the solution during the experiments. The experiments were controlled with a VMP3 potentiostat and EC-Lab software (Bio-Logic Science Instruments).

Conflict of Interest: The authors declare no competing financial interest.

Supporting Information Available: SEM images of commercial Li_2O_2 and Vulcan XC72 electrodes prefilled with Li_2O_2; OEMS analysis during charge of a ^{13}C electrode prefilled with Li_2O_2; electrochemical characterization of TiN nanopowder for ORR and OER; electrochemical impedance spectroscopy of carbon and TiN during the first galvanostatic cycles in Li−O_2 cells; XRD and SEM images of TiC-A and TiC-B nanopowders; XPS of TiN nanopowder; OEMS comparison of TiC-B electrode in DMSO and TEGDME electrolytes; CVs of Fc/Fc+ couple on TiC's; results and experimental details of iodometric titrations for determining the purity of Li_2O_2. This material is available free of charge *via* the Internet at http://pubs.acs.org.

Acknowledgment. NSERC is acknowledged by L.F.N. for a Canada Research Chair, and B.D.A. and R.B. for a graduate scholarship (CGS-D). B.D.A. and R.B. also thank the Waterloo Institute of Technology for WIN fellowships. C.R. thanks CNPq for a fellowship. This work was supported in part by the Joint Center for Energy Storage Research (JCESR), an Energy Innovation Hub funded by the U.S. Department of Energy (DOE), Office of Science, Basic Energy Sciences (electrochemical and TEM) and as part of the Chemical Imaging Initiative conducted under the Laboratory Directed Research and Development Program at Pacific Northwest National Laboratory (PNNL). The (S)TEM work was conducted in the William R. Wiley Environmental Molecular Sciences Laboratory (EMSL), a national scientific user facility sponsored by DOE's Office of Biological and Environmental Research and located at PNNL. PNNL, a multiprogram national laboratory, is operated by Battelle for the Department of Energy under Contract DE-AC05-76RLO1830. We thank Dipan Kundu (UW) for his assistance with the iodometric titrations.

REFERENCES AND NOTES

1. Black, R.; Adams, B.; Nazar, L. F. Non-Aqueous and Hybrid Li-O_2 Batteries. *Adv. Energy Mater.* **2012**, *2*, 801–815.
2. Lu, J.; Li, L.; Park, J.-B.; Sun, Y.-K.; Wu, F.; Amine, K. Aprotic and Aqueous Li−O_2 Batteries. *Chem. Rev.* **2014**, *114*, 5611–5640.
3. Lu, Y.-C.; Gallant, B. M.; Kwabi, D. G.; Harding, J. R.; Mitchell, R. R.; Whittingham, M. S.; Shao-Horn, Y. Lithium-Oxygen Batteries: Bridging Mechanistic Understanding and Battery Performance. *Energy Environ. Sci.* **2013**, *6*, 750–768.
4. Jung, H.-G.; Jeong, Y. S.; Park, J.-B.; Sun, Y.-K.; Scrosati, B.; Lee, Y.-J. Ruthenium-Based Electrocatalysts Supported on Reduced Graphene Oxide for Lithium-Air Batteries. *ACS Nano* **2013**, *7*, 3532–3539.
5. Adams, B. D.; Radtke, C.; Black, R.; Trudeau, M. L.; Zaghib, K.; Nazar, L. F. Current Density Dependence of Peroxide Formation in the Li−O_2 Battery and Its Effect on Charge. *Energy Environ. Sci.* **2013**, *6*, 1772–1778.
6. Peng, Z.; Freunberger, S.; Hardwick, L. J.; Chen, Y.; Giordani, V.; Bardé, F.; Novák, P.; Graham, D.; Tarascon, J.-M.; Bruce, P. G. Oxygen Reactions in a Non-Aqueous Li^+ Electrolyte. *Angew. Chem., Int. Ed.* **2011**, *50*, 6351–6355.
7. McCloskey, B. D.; Scheffler, R.; Speidel, A.; Bethune, D. S.; Shelby, R. M.; Luntz, A. C. On the Efficacy of Electrocatalysis in Nonaqueous Li-O_2 Batteries. *J. Am. Chem. Soc.* **2011**, *133*, 18038–18041.
8. Freunberger, S. A.; Chen, Y.; Drewett, N. E.; Hardwick, L. J.; Bardé, F.; Bruce, P. G. The Lithium−Oxygen Battery with Ether-Based Electrolytes. *Angew. Chem., Int. Ed.* **2011**, *50*, 8609–8613.
9. Freunberger, S. A.; Chen, Y.; Peng, Z.; Griffin, J. M.; Hardwick, L. J.; Bardé, F.; Novák, P.; Bruce, P. G. Reactions in the Rechargeable Lithium-O_2 Battery with Alkyl Carbonate Electrolytes. *J. Am. Chem. Soc.* **2011**, *133*, 8040–8047.
10. Bryantsev, V. S.; Giordani, V.; Walker, W.; Blanco, M.; Zecevic, S.; Sasaki, K.; Uddin, J.; Addison, D.; Chase, G. V. Predicting Solvent Stability in Aprotic Electrolyte Li-Air Batteries: Nucleophilic Substitution by the Superoxide Anion Radical ($O_2^{\bullet-}$). *J. Phys. Chem. A* **2011**, *115*, 12399–12409.
11. Mccloskey, B. D.; Bethune, D. S.; Shelby, R. M.; Girishkumar, G.; Luntz, A. C. Solvents' Critical Role in Nonaqueous Lithium-Oxygen Battery Electrochemistry. *J. Phys. Chem. Lett.* **2011**, 1161–1166.
12. Chen, Y.; Freunberger, S. A.; Peng, Z.; Bardé, F.; Bruce, P. G. The Li-O_2 Battery with a Dimethylformamide Electrolyte. *J. Am. Chem. Soc.* **2012**, *134*, 7952–7957.
13. Thotiyl, M. M. O.; Freunberger, S. A.; Peng, Z.; Bruce, P. G. The Carbon Electrode in Nonaqueous Li−O_2 Cells. *J. Am. Chem. Soc.* **2013**, *135*, 494–500.
14. Itkis, D. M.; Semenenko, D.; Kataev, E. Y.; Belova, A. I.; Neudachina, V. S.; Sirotina, A. P.; Hävecker, M.; Teschner, D.; Knop-Gericke, A.; Dudin, P.; *et al.* Reactivity of Carbon in Lithium-Oxygen Battery Positive Electrodes. *Nano Lett.* **2013**, *13*, 4697–4701.
15. Lu, J.; Lei, Y.; Lau, K. C.; Luo, X.; Du, P.; Wen, J.; Assary, R. S.; Das, U.; Miller, D. J.; Elam, J. W.; *et al.* Nanostructured Cathode Architecture for Low Charge Overpotential in Lithium-Oxygen Batteries. *Nat. Commun.* **2013**, *4*, 2383.
16. Peng, Z.; Freunberger, S. A.; Chen, Y.; Bruce, P. G. A Reversible and Higher-Rate Li-O_2 Battery. *Science* **2012**, *337*, 563–566.
17. Chen, Y.; Freunberger, S. A.; Peng, Z.; Fontaine, O.; Bruce, P. G. Charging a Li−O_2 Battery Using a Redox Mediator. *Nat. Chem.* **2013**, *5*, 489–494.
18. Thotiyl, M. M. O.; Freunberger, S. A.; Peng, Z.; Chen, Y.; Liu, Z.; Bruce, P. G. A Stable Cathode for the Aprotic Li−O_2 Battery. *Nat. Mater.* **2013**, *12*, 1050–1056.
19. Zhao, G.; Mo, R.; Wang, B.; Zhang, L.; Sun, K. Enhanced Cyclability of Li−O_2 Batteries Based on TiO_2 Supported Cathodes with No Carbon or Binder. *Chem. Mater.* **2014**, *26*, 2551–2556.
20. Avasarala, B.; Haldar, P. Electrochemical Oxidation Behavior of Titanium Nitride Based Electrocatalysts Under PEM Fuel Cell Conditions. *Electrochim. Acta* **2010**, *55*, 9024–9034.
21. Ham, D. J.; Lee, J. S. Transition Metal Carbides and Nitrides as Electrode Materials for Low Temperature Fuel Cells. *Energies* **2009**, *2*, 873–899.
22. He, P.; Wang, Y.; Zhou, H. Titanium Nitride Catalyst Cathode in a Li−Air Fuel Cell with an Acidic Aqueous Solution. *Chem. Commun.* **2011**, *47*, 10701–10703.
23. Park, J.; Jun, Y.-S.; Lee, W.-R.; Gerbec, J. A.; See, K. A.; Stucky, G. D. Bimodal Mesoporous Titanium Nitride/Carbon Microfibers as Efficient and Stable Electrocatalysts for Li−O_2 Batteries. *Chem. Mater.* **2013**, *25*, 3779–3781.
24. Li, F.; Ohnishi, R.; Yamada, Y.; Kubota, J.; Domen, K.; Yamada, A.; Zhou, H. Carbon Supported TiN Nanoparticles: An Efficient Bifunctional Catalyst for Non-Aqueous Li−O_2 Batteries. *Chem. Commun.* **2013**, *49*, 1175–1177.
25. Kenney, M. J.; Gong, M.; Li, Y.; Wu, J. Z.; Feng, J.; Lanza, M.; Dai, H. High-Performance Silicon Photoanodes Passivated with Ultrathin Nickel Films for Water Oxidation. *Science* **2013**, *342*, 836–840.
26. Nasybulin, E.; Xu, W.; Engelhard, M. H.; Nie, Z.; Burton, S. D.; Cosimbescu, L.; Gross, M. E.; Zhang, J. Effects of Electrolyte Salts on the Performance of Li−O_2 Batteries. *J. Phys. Chem. C* **2013**, *117*, 2635–2645.
27. Lu, Y.-C.; Gasteiger, H. A.; Parent, M. C.; Chiloyan, V.; Shao-Horn, Y. The Influence of Catalysts on Discharge and Charge Voltages of Rechargeable Li−Oxygen Batteries. *Electrochem. Solid-State Lett.* **2010**, *13*, A69–A72.
28. Harding, J. R.; Lu, Y.-C.; Tsukada, Y.; Shao-Horn, Y. Evidence of Catalyzed Oxidation of Li_2O_2 for Rechargeable Li−Air Battery Applications. *Phys. Chem. Chem. Phys.* **2012**, *14*, 10540–10546.
29. Meini, S.; Tsiouvaras, N.; Schwenke, K. U.; Piana, M.; Beyer, H.; Lange, L.; Gasteiger, H. A. Rechargeability of Li−Air Cathodes Pre-Filled with Discharge Products Using an Ether-Based Electrolyte Solution: Implications for Cycle-Life of Li−Air Cells. *Phys. Chem. Chem. Phys.* **2013**, *15*, 11478–11493.
30. Beyer, H.; Meini, S.; Tsiouvaras, N.; Piana, M.; Gasteiger, H. A. Thermal and Electrochemical Decomposition of Lithium Peroxide in Non-Catalyzed Carbon Cathodes for

Li−Air Batteries. *Phys. Chem. Chem. Phys.* **2013**, *15*, 11025–11037.
31. Ganapathy, S.; Adams, B. D.; Stenou, G.; Anastasaki, M. S.; Goubitz, K.; Miao, X.-F.; Nazar, L. F.; Wagemaker, M. The Nature of Li_2O_2 Oxidation in a Li-O_2 Battery Revealed by Operando X-Ray Diffraction. *J. Am. Chem. Soc.* **2014**, 10.1021/ja508794r.
32. Meini, S.; Solchenbach, S.; Piana, M.; Gasteiger, H. A. The Role of Electrolyte Solvent Stability and Electrolyte Impurities in the Electrooxidation of Li_2O_2 in Li-O_2 Batteries. *J. Electrochem. Soc.* **2014**, *161*, A1306–A1314.
33. McCloskey, B. D.; Speidel, A.; Scheffler, R.; Miller, D. C.; Viswanathan, V.; Hummelshøj, J. S.; Nørskov, J. K.; Luntz, A. C. Twin Problems of Interfacial Carbonate Formation in Nonaqueous Li−O2 Batteries. *J. Phys. Chem. Lett.* **2012**, *3*, 997–1001.
34. Yang, J.; Zhai, D.; Wang, H. H.; Lau, K. C.; Schlueter, J. A.; Du, P.; Myers, D. J.; Sun, Y. K.; Curtiss, L. A.; Amine, K. Evidence for Lithium Superoxide-like Species in the Discharge Product of a Li-O_2 Battery. *Phys. Chem. Chem. Phys.* **2013**, *15*, 3764–3771.
35. Avasarala, B.; Haldar, P. On the Stability of TiN-Based Electrocatalysts for Fuel Cell Applications. *Int. J. Hydrogen Energy* **2011**, *36*, 3965–3974.
36. Gavarini, S.; Bes, R.; Millard-Pinard, N.; Cardinal, S.; Peaucelle, C.; Perrat-Mabilon, A.; Garnier, V.; Gaillard, C. A Comparative Study of TiN and TiC: Oxidation Resistance and Retention of Xenon at High Temperature and Under Degraded Vacuum. *J. Appl. Phys.* **2011**, *109*, 014906(1−9).
37. Wasche, R.; Klaffke, D. Ceramic Particulate Composites in the System SiC−TiC−TiB_2 the System SiC−TiC−TiB_2 Sliding against SiC and Al_2O_3 Under Water. *Tribol. Int.* **1999**, *32*, 197–206.
38. Komratov, G. N. The Oxidation Kinetics of Titanium Carbide, Nitride, and Carbonitride Powders in Air. *Powder Metall. Met. Ceram.* **1997**, *36*, 510–514.
39. Adams, B. D.; Black, R.; Williams, Z.; Fernandes, R.; Cuisinier, M.; Jaemstorp Berg, E.; Novak, P.; Murphy, G. K.; Nazar, L. F. Towards a Stable Organic Electrolyte for the Lithium Oxygen Battery. *Adv. Energy Mater.* **2014**, 10.1002/aenm.201400867.
40. McCloskey, B. D.; Valery, A.; Luntz, A. C.; Gowda, S. R.; Wallraff, G. M.; Garcia, J. M.; Mori, T.; Krupp, L. E. Combining Accurate O_2 and Li_2O_2 Assays to Separate Discharge and Charge Stability Limitations in Nonaqueous Li−O_2 Batteries. *J. Phys. Chem. Lett.* **2013**, *4*, 2989–2993.
41. Tsiouvaras, N.; Meini, S.; Buchberger, I.; Gasteiger, H. A. A Novel On-Line Mass Spectrometer Design for the Study of Multiple Charging Cycles of a Li-O_2 Battery. *J. Electrochem. Soc.* **2013**, *160*, A471–A477.
42. Garsuch, R. R.; Le, D.-B.; Garsuch, A.; Li, J.; Wang, S.; Farooq, A.; Dahn, J. R. Studies of Lithium-Exchanged Nafion as an Electrode Binder for Alloy Negatives in Lithium-Ion Batteries. *J. Electrochem. Soc.* **2008**, *155*, A721–A724.